Biochimica et Biophysica Acta 1837 (2014) 1305–1315

Contents lists available at ScienceDirect

Biochimica et Biophysica Acta

journal homepage: www.elsevier.com/locate/bbabio

The dynamic complex of cytochrome c_6 and cytochrome *f* studied with paramagnetic NMR spectroscopy

Irene Díaz-Moreno [a], Rinske Hulsker [b], Pavol Skubak [b], Johannes M. Foerster [c], Davide Cavazzini [d], Michelina G. Finiguerra [b], Antonio Díaz-Quintana [a], Blas Moreno-Beltrán [a], Gian-Luigi Rossi [d], G. Matthias Ullmann [c], Navraj S. Pannu [b], Miguel A. De la Rosa [a], Marcellus Ubbink [b,*]

[a] *Instituto de Bioquímica Vegetal y Fotosíntesis, Universidad de Sevilla-CSIC, Avda. Américo Vespucio 49, Sevilla 41092, Spain*
[b] *Institute of Chemistry, Leiden University, Einsteinweg 55, 2333 CC Leiden, The Netherlands*
[c] *Computational Biochemistry, University of Bayreuth, Universitätsstrasse 30, 95447 Bayreuth, Germany*
[d] *Department of Life Sciences, Laboratory of Biochemistry, Molecular Biology and Bioinformatics, Parco Area delle Scienze 23/a, University of Parma, 43124 Parma, Italy*

ARTICLE INFO

Article history:
Received 27 January 2014
Received in revised form 13 March 2014
Accepted 16 March 2014
Available online 28 March 2014

Keywords:
Electron transfer
Photosynthesis
Crystallography
Paramagnetic relaxation enhancement
Monte-Carlo modelling
Protein interaction

ABSTRACT

The rapid transfer of electrons in the photosynthetic redox chain is achieved by the formation of short-lived complexes of cytochrome b_6f with the electron transfer proteins plastocyanin and cytochrome c_6. A balance must exist between fast intermolecular electron transfer and rapid dissociation, which requires the formation of a complex that has limited specificity. The interaction of the soluble fragment of cytochrome *f* and cytochrome c_6 from the cyanobacterium *Nostoc* sp. PCC 7119 was studied using NMR spectroscopy and X-ray diffraction. The crystal structures of wild type, M58H and M58C cytochrome c_6 were determined. The M58C variant is an excellent low potential mimic of the wild type protein and was used in chemical shift perturbation and paramagnetic relaxation NMR experiments to characterize the complex with cytochrome *f*. The interaction is highly dynamic and can be described as a pure encounter complex, with no dominant stereospecific complex. Ensemble docking calculations and Monte-Carlo simulations suggest a model in which charge–charge interactions pre-orient cytochrome c_6 with its haem edge toward cytochrome *f* to form an ensemble of orientations with extensive contacts between the hydrophobic patches on both cytochromes, bringing the two haem groups sufficiently close to allow for rapid electron transfer. This model of complex formation allows for a gradual increase and decrease of the hydrophobic interactions during association and dissociation, thus avoiding a high transition state barrier that would slow down the dissociation process.

1. Introduction

Protein complex formation is at least a two-step process [3] in which the formation of a final, well-defined complex – dominated by short-range interactions – entails the initial formation of a dynamic encounter complex. The lifetime of the protein complex is determined by the dissociation rate. Highly transient complexes, with lifetimes on the order of milliseconds, exhibit moderate or low binding affinities, with dissociation constants in the μM–mM range. Electron transfer (ET^1) reactions mediated by soluble redox proteins exchanging electrons between large membrane complexes in photosynthesis and respiration are excellent examples of transient interactions. The purpose of the protein complex formation in these cases is two-fold. A complex must be formed that is sufficiently specific to allow rapid electron transfer and at the same time the complex needs a high dissociation rate to enable rapid turn-over in order not to limit the flow of electrons through the redox chain. The electron transfer rate is exponentially dependent on the distance between the redox centres. Thus, bringing the centres in close approximation (<16 Å) [4] is essential, but the formation of a well-defined complex is not required if multiple orientations exist in which ET can occur. In fact, such a specific complex is not desirable from the point of view of fast dissociation, because a well-defined state has a lower free energy than all similar states and thus a higher transition state energy to be overcome to dissociate. In other words, high specificity opposes rapid turnover. The study of transient complexes enables the understanding of the biophysical mechanisms that exist to reach the right compromise between these two properties of a complex.

Abbreviations: Cb6f, Cytochrome b_6f; Cc6, Cytochrome c_6; Cf, Cytochrome *f*; ET, Electron transfer; PRE, Paramagnetic relaxation enhancement; MTS, (1-Acetyl-2,2,5,5-tetramethyl-3-pyrroline-3-methyl)-methanethiosulfonate; MTSL, (1-Oxyl-2,2,5,5-tetramethyl-3-pyrroline-3-methyl)-methanethiosulfonate

* Corresponding author at: Tel.: +31 715274628.
E-mail addresses: idiazmoreno@us.es (I. Díaz-Moreno), hulsker_rinske@yahoo.co.uk (R. Hulsker), p.skubak@chem.leidenuniv.nl (P. Skubak), johannes.foerster@uni-bayreuth.de (J.M. Foerster), davide.cavazzini@unipr.it (D. Cavazzini), mfinig@hotmail.com (M.G. Finiguerra), qzaida@us.es (A. Díaz-Quintana), joseblas.moreno@ibvf.csic.es (B. Moreno-Beltrán), gianluigi.rossi@unipr.it (G.-L. Rossi), Matthias.Ullmann@uni-bayreuth.de (G.M. Ullmann), raj@chem.leidenuniv.nl (N.S. Pannu), marosa@us.es (M.A. De la Rosa), m.ubbink@chem.leidenuniv.nl (M. Ubbink).

http://dx.doi.org/10.1016/j.bbabio.2014.03.009
0005-2728/

In oxygenic photosynthesis, the ET from the cytochrome b_6f (Cb6f) complex to Photosystem I (PSI) – both membrane-embedded complexes – is carried out by two soluble metalloproteins, plastocyanin (Pc) and cytochrome c_6 (Cc6) [5–8]. Most cyanobacteria and green algae synthesize either Pc or Cc6, depending on the availability of copper and iron, their respective cofactor metals [9,10]. Higher plants only contain Pc, although a Cc6-like protein has been identified in *Arabidopsis* [11], but it is unable to transfer electrons to PSI [12].

The hetero-oligomeric Cb6f complex contains eight tightly bound polypeptide subunits that couple the ET to proton translocation, generating a proton electrochemical potential gradient necessary for ATP synthesis. The three-dimensional crystal structure has been determined for the Cb6f complex from the green alga *Chlamydomonas reinhardtii* [13], the cyanobacteria *Mastigocladus laminosus* [14] and *Nostoc* sp. PCC 7120 [15]. The main difference between the cyanobacterial Cb6f crystallographic structures is the acetylation of the *Nostoc* Rieske Fe–S protein at the N terminus, a post-translational modification unprecedented in cyanobacterial membrane and ET proteins [15]. Cytochrome *f* (Cf) is a subunit of the Cb6f complex, anchored to the thylakoid membrane by a C-terminal transmembrane helix leaving a 28-kDa soluble portion exposed to the lumen with a clear two-domain structure. The large domain harbours the haem and the small domain possesses a patch of charged residues. Cf is considered an unusual *c*-type cytochrome because of its β-sheet structure, elongated form and particular haem axial coordination with the amino group of the N-terminus, residue Tyr1 [13–17].

Cc6 is a more typical 10-kDa single haem *c*-type cytochrome with the cofactor covalently bound to the cysteine residues in a CXXCH motif. The Fe atom is hexacoordinated with His and Met residues acting as axial ligands, as revealed by the available cyanobacterial and green algal Cc6 structures [18–22]. One of the most important functional characteristic of Cc6 is its midpoint redox potential (E_m) around +335 mV at physiological pH value, with the exception of that present in plants whose E_m is substantially lower (*ca.* +100 mV) despite having the same axial ligands [23]. This finding can be partly explained by the replacement of a highly conserved Gln in cyanobacterial Cc6 by a Val residue in the plant Cc6-like protein, which regulates the Fe–S(Met) bond stability and causes a 100 mV-drop in the E_m [20,24]. A more drastic E_m change occurs when the sixth axial ligand Met is substituted by His, leading to inhibition of both the spontaneous self-reduction of Cc6 mutant and its reduction by the Cb6f complex [25].

Cc6-involving physiological interactions have been extensively studied in recent years as a model to understand the nature of protein–protein interactions in ET chains. The Cc6–PSI interaction from *Nostoc* has been well-characterized from the structural and functional point of view [26–30]. Fast-kinetics studies combined with Brownian dynamics using a *Chlamydomonas* Zn–Cc6 derivative and Cf have been reported [31,32], concluding that the nature of this complex is dynamic and that hydrophobic contacts are important. Two NMR-based structural approaches using haem proteins from different cyanobacterial sources also suggest that the binding site on *Nostoc* Cc6 involves the predominantly hydrophobic patch surrounding the Cf haem [33,34]. *In silico* data on *Chlamydomonas* Cc6–Cf complex show not only the relevance of hydrophobic and electrostatic interactions in bringing both haem proteins sufficiently close to allow efficient ET [35,36], but also the key role of the Cf small domain in binding to Cc6, suggesting that Cc6 explores different positions on Cf [37].

Here, experimental approaches using NMR spectroscopy are combined with charge-driven docking simulations to study the molecular recognition processes in ET complexes, using the physiological *Nostoc* Cc6–Cf interaction as a model system. Our paramagnetic relaxation enhancement (PRE) NMR data are not compatible with a well-defined Cc6–Cf complex. The complex is best described by a highly dynamic ensemble, first formed by electrostatic pre-orientation and stabilized mainly by hydrophobic contacts.

2. Materials and methods

2.1. Mutagenesis

The expression vector pEAC-WT for wt Cc6 from *Nostoc* sp. PCC 7119 [38] was used as the template for site-directed mutagenesis to obtain the M58H and M58C variants using the QuikChange PCR protocol (Stratagene, La Jolla, CA). The following primer pairs were used: 5′ CGGTAAGAACGCCCACCCTGCTTTCAAAGG and its complement for M58H and 5′ CGGTAAGAACGCCTGCCCTGCTTTCAAAGG and its complement for M58C. For the introduction of Cys residues in Cf, the pEAF-wt [39] expression plasmid encoding the soluble domain of Cf from *Nostoc* sp. PCC7119 was used as template. The single-cysteine variants Q7C, A63C, N71C, Q104C and S192C have been described before [40,41]. All constructs were verified by DNA sequencing.

2.2. Protein production and purification

Uniformly ^{15}N-labelled *Nostoc* sp. PCC 7119 Cc6 wt and its mutants were produced as described before [26] in *Escherichia coli* JM109 cells co-transformed with pEAC-WT [38] and pEC86 [42]. Culture conditions and protein purification methods were as reported previously [26,33]. Protein concentrations were determined by absorption spectrophotometry using a ε_{553} of 26.2 mM^{-1} cm^{-1} for the ferrous form of Cc6 wt [38], a ε_{554} of 20.8 mM^{-1} cm^{-1} for the ferrous form of M58H and a ε_{540} of 7.2 mM^{-1} cm^{-1} for the ferric form of M58C mutant. The Cc6 wt ε_{278} was estimated using protein concentration values from Bradford assays. A A_{278}/A_{553} ratio of 1.05 of the wt ferrous Cc6 indicated sufficient purity for characterization by NMR.

To obtain a high yield of holo-Cf and promote the correct insertion of the haem group, *E. coli* strain MV1190 (Bio-Rad) was co-transformed with plasmids pEC86 and (mutated) pEAF plasmid. The cells were plated on Lysogeny Broth (LB) medium plates and incubated at 37 °C for 24 h. All media were supplemented with 20 mg/L ampicillin and chloramphenicol. Several pre-cultures were prepared in 100 mL flasks with 20 mL of LB medium and incubated at 37 °C and 250 rpm for 5–6 h. The pre-cultures with the highest OD_{600} were used to inoculate 1.7 L (in 2 L Erlenmeyer flasks) of LB, ratio 1:100. The cultures were incubated at 25 °C and 150 rpm under semi-anaerobic conditions and high antibiotic pressure by adding further ampicillin and chloramphenicol after 20 h and 40 h. Expression was induced 20 h after the inoculation of the large culture using 1 mM IPTG (isopropyl-β-thiogalactopyranoside). More than 80 h after the induction the cultures appeared brown because of the presence of Cf. The cells were harvested by centrifugation and the periplasmic fraction was extracted by osmotic shock. The pink water fraction (about 200 mL *per* 1.7 L of culture), was dialyzed against 2 L of 5 mM Tris–HCl buffer, pH 8 and 3 mM dithiothreitol (DDT). The yield in the periplasmatic fraction was 10 mg/L of culture of protein for N71C and Q7C and 5 mg/L for Q104C, S192C and A63C. The resulting dialysate was cleared by centrifugation and loaded on a DEAE column equilibrated in the same buffer. Elution was performed with a gradient of 20–500 mM NaCl and 3 mM DTT. The fraction containing the Cf was concentrated and loaded on a gel-filtration (G75 Superdex) column and eluted in the same buffer containing 150 mM NaCl. The protein fractions were pooled, concentrated, dialyzed against 5 mM MES, pH 6 and 3 mM DTT and loaded on a DEAE column equilibrated in the same buffer. The Cf was eluted with a gradient of 0–500 mM NaCl. Pure fractions showed a A_{280}/A_{556} of 1.3 under reducing conditions. Protein concentrations were determined by optical spectroscopy using ε_{419} of 85.5 mM^{-1} cm^{-1} for Cc6 M58C and ε_{556} = 31.5 mM^{-1} cm^{-1} for reduced Cf [39].

2.3. Labelling of Cf with spin labels

For attachment of spin label to Cf, DTT was first removed by ultrafiltration (Amicon, MW cut-off 10 kDa). The protein was subsequently

exchanged to 10 mM sodium phosphate, pH 6.0 and concentrated to ~40 μM. The protein was oxidized by a 100-fold excess of $K_3[Fe(CN)_6]$ and a 10-fold excess was added of either MTSL [(1-oxyl-2,2,5,5-tetramethyl-3-pyrroline-3-methyl)-methanethiosulfonate] or MTS [(1-acetyl-2,2,5,5-tetramethyl-3-pyrroline-3-methyl)-methanethiosulfonate] (TRC, North York, Ontario, Canada). Stock solutions of 0.1 M MTS(L) in DMSO were used. The protein solution was kept for 2 h at RT and O/N at 4° after which the excess $K_3[Fe(CN)_6]$ and MTS(L) were removed by ultrafiltration.

2.4. Electrochemistry

The redox potential value for the haem group in each Cc6 wt and mutants was determined as reported previously [38], for which the differential absorbance changes at 553 minus 570 nm were followed. Menadione, diaminodurol and ρ-benzoquinone, at 20 μM final concentration, were used as redox mediators. Errors in the experimental determinations were less than 20 mV.

2.5. Crystallization and data collection

Crystals were obtained with the sitting drop method. The final protein concentration was 10 mg/mL in the following solutions: Cc6 wt: 0.1 M Tris/HCl pH 7.0, 2.3 M ammonium sulphate, 0.1 M lithium sulphate; Cc6 M58H: 0.1 M Tris/HCl pH 8.0, 2.5 M ammonium sulphate, 0.1 M lithium sulphate; and Cc6 M58C: 0.1 M citrate pH 5.0, 2.5 M ammonium sulphate. The crystals were frozen and diffraction data for the wild type and M58H crystals were collected at the BM16 beamline of the ESRF synchrotron on a MAR 165 CCD detector at the peak wavelength of the iron (1.5418 Å), whereas M58C crystals were collected in-house on an Enraf-Nonius FR591 generator and MAD 345 image plate detector. All crystals were collected with a 1.0° oscillation at 100 K. For the wild type crystals 360 images were collected, for the M58H crystals 230 and for the M58C crystals 200 images. All data sets were processed by MOSFLM [43] and SCALA [44] from CCP4 [45].

Molecular replacement for the wild type Cc6 structure was unsuccessful due to the presence of translational non-crystallographic symmetry, as noted by a large off-origin peak in the Patterson map. However, the anomalous signal from the intrinsic iron atoms was sufficient for structure determination by SAD phasing. The CRANK [46] software pipeline was used to solve the structure and CRUNCH2 was used [47] for substructure detection, BP3 [46] for heavy atom refinement, and density modification by DM [48] estimates. Automated model building with ARP/wARP [49] using the iterative refinement with the SAD target [50] in REFMAC [51] provided a good quality model of the structure consisting of 483 backbone residues, 478 of which were (correctly) docked in the 6 wild type molecules present in the asymmetric unit. Some of the chains traced missed several residues from either the *C*- or *N*-terminus, however, one chain contained all the residues fitting well in the electron density. The haem group was fitted manually into the chain that was built completely at this stage. The resulting completely built Cc6 molecule was superimposed on the five other cytochrome molecules present in the asymmetric unit to fit in any missed residues present in the density as well as the other haem groups. The model obtained in this way was refined by REFMAC5 with tight NCS restraints. Manual corrections to the model were performed with XtalView [52], followed by refinement with REFMAC with loose NCS restraints.

The point mutation M58C crystal was isomorphic to the wild type crystal, thus the final wild type model was used as a starting model in the refinement of the M58C mutant. The structure of M58H Cc6 was solved by molecular replacement using the wild type structure and contained two molecules in the asymmetric unit. Manual fitting and refinement of both mutant structures was done with COOT [1] and REFMAC. Data collection and refinement statistics are reported in Table 1. The coordinates have been deposited in the protein data bank with PDB IDs: 4GYD for wildtype, 4H0J for M58C, and 4H0K for M58H Cc6.

2.6. NMR spectroscopy and data analysis

Cc6 wt and M58C mutant protein solutions were concentrated to the required volume by ultrafiltration methods (Amicon, YM3 membrane) and exchanged into 10 mM sodium phosphate, pH 6.0, H_2O/D_2O 95:5 (v/v) solutions. The soluble domain of Cf was concentrated using an Amicon YM10 membrane and exchanged into 10 mM sodium phosphate, pH 6.0, 3 mM sodium ascorbate, H_2O/D_2O 95:5 solutions. A 3.7 mM ferrous Cf stock solution with a A_{278}/A_{556} ratio of 0.9 was used. Cf was kept in a reduced form with a few equivalents of sodium ascorbate and was stable in this form for days. The ferric form was prepared by the addition of a 5-fold excess of potassium ferricyanide ($K_3[Fe(CN)_6]$) followed by gel filtration (Amersham Biosciences Superdex G75) to remove ferrocyanide. Complete oxidation was verified by the disappearance of the absorption band at 556 nm. Then, a 2.0 mM ferric Cf stock solution was prepared.

All NMR experiments were performed on a Bruker DMX 600 NMR spectrometer with a TXI or TCI-cryo triple resonance probehead operating at 298 K. The ^1H and ^{15}N assignments of the backbone amide resonances from ferric *Nostoc* M58C Cc6 mutant (Table S1) were elucidated by recording 2D $^1H,^{15}N$ HSQC-NOESY with 150 ms mixing time and 2D $^1H,^{15}N$ HSQC-TOCSY with 80-ms mixing time spectra. The effects of complex formation on M58C were followed by acquiring 2D $^1H,^{15}N$ HSQC spectra during titrations of aliquots of Cf stock solutions into a solution of 0.2 mM ^{15}N-labelled M58C. For the measurements of PRE, samples contained 0.3 mM ^{15}N M58C Cc6 and 0.1 mM Cf-MTS(L).

All data processing was performed with AZARA 2.7 (www2.ccpn.ac.uk/azara), and spectral analysis was performed with Ansig [53,54]. The spectra were calibrated against the internal standard [^{15}N]acetamide (0.5 mM).

Titration curves were obtained by plotting chemical-shift perturbations ($\Delta\delta_{Bind}$) against the molar ratio of Cf and Cc6 M58C for the most strongly affected signals. Non-linear least squares fits to a 1:1 binding model [55] were performed in Origin 8.0 (Microcal Inc.). The chemical-shift perturbations (CSP) observed in the complex M58C-Cf with 3 eq. of Cf were extrapolated to 100% bound for all residues using the K_a obtained from the fits. The average chemical-shift perturbation ($\Delta\delta_{avg}$) of each amide was calculated using the following equation: $\Delta\delta_{avg} = (((\Delta\delta_N / 5)^2 + (\Delta\delta_H)^2) / 2)^{1/2}$ in which $\Delta\delta_N$ is the change in the ^{15}N chemical shift, and $\Delta\delta_H$ is the change in the ^1H chemical shift when the protein is 100% bound to Cf.

PREs were derived from the ratio of intensities in the spectra from paramagnetic and diamagnetic samples and converted into distances, as described [56,57]. The correlation time assumed for the Cf and Cc6 complex was 20 ns. PREs are only observed for the fraction of Cc6 that is bound to Cf. The binding is in fast exchange, so the PREs are weighted by the fraction bound. Therefore, the PREs were extrapolated to the 100% bound state of Cc6 for docking calculations.

2.7. Ensemble docking

Cf from *Nostoc* sp. PCC 7120 is identical to that of PCC 7119. The crystal structure of Cf of the former species from PDB ID 2ZT9 [15], residues 1–254, was modified to introduce Cys residues and MTSL spin labels for Gln 7, Ala 63, Asn 71, Gln 104 and Ser 192. Each spin label was built in four orientations, to represent its mobility [58]. For Cc6 the structure from the wt protein from *Nostoc* sp. PCC 7119 (this study) was used. Protons were added to both structures.

In the combined single structure/ensemble docking, first the experimental distances were assigned as restraints between the oxygens of the four MTSL conformers of a spin label and an amide proton of a single copy of Cc6. During the docking, the spin labels were free to rotate. After docking, the distances were measured in the lowest energy structure

Table 1
Data collection and refinement statistics for Cc6 crystals.

	Wild type	M58C	M58H
Space group	P 21 21 2	P 21 21 2	P 32 2 1
Cell dimensions			
a, b, c (Å)	77.72, 79.80, 80.15	78.82, 80.16, 80.15	60.37, 60.37, 95.37
Resolution (Å)	18.00–1.80 (1.90–1.80)[a]	28.33–2.00 (2.10–2.00)[a]	35.23–1.95 (2.06–1.95)[a]
R_{pim}	0.026 (0.113)	0.021 (0.129)	0.022 (0.221)
I/σI	27.0 (10.1)	23.8 (6.3)	18.8 (3.4)
Completeness (%)	97.3 (94.0)	98.6 (93.8)	99.7 (99.1)
Redundancy	3.4 (2.4)	7.5 (5.2)	12.4 (11.4)
N° unique reflections	44311	32761	14317
N° molecules in ASU	6	6	2
R_{work}/R_{free}	0.182/0.216	0.207/0.246	0.213/0.268
R.m.s. deviations			
Bond lengths (Å)	0.021	0.017	0.018
Bond angles (°)	1.92	1.72	1.96
Ramachandran favored[b]	90.7%	93.7%	91.6%
Ramachandran outliers[b]	0.40%	0.20%	2.99%

[a] Values from the highest resolution shell are given in brackets.
[b] As defined by COOT.

and converted back to PREs. These back-calculated values were subtracted from the experimental PREs and the difference served as the input for the ensemble docking. Five copies of Cc6 were used and the input PREs were assigned as distance restraints between the nitroxy oxygens and the five copies of the amide protons simultaneously. All averaging was done using the sixth power of the distance. The Cf structure resulting from the single-structure docking was used as the input for the ensemble docking and the spin label orientations were fixed during the ensemble docking. Because of this, the compatibility between the two stages of the docking is ensured. The top ten ensembles were used to calculate the average distance violations. To ensure that the ensemble docking is not strongly influenced by the starting structure, the ensemble docking was repeated several times using the next best structure from the single structure docking as input and repeating the entire procedure. These results yielded the average distance violation and error margins (SD) shown in Fig. 3. For the 0% and 100% ensemble fractions, only a single-structure or ensemble docking was used, respectively, and the experimental PREs served as the restraints. All docking calculations treated the proteins as rigid bodies, using the rigid body dynamic routine in XPLOR-NIH [59]. PREs were divided into three classes, as described before [57]. Resonances that were not significantly affected yielded a distance that served as lower bound only. Resonances that were affected but not completely broadened yielded a distance (with and upper and lower bound of 3 Å in the docking calculations) and signals that were strongly affected (PRE of 100% bound state > 200 s^{-1}) or completely broadened provided only an upper bound distance. The distance violations were defined as the difference between the target distance or range and the back-calculated value. For the first and the third class, this criterion means a violation for values below or above the distance bound, respectively, and for the second class the violations are the absolute difference between target and back-calculated values (so the error margins were not considered for the violation).

2.8. Monte Carlo docking

In the Monte-Carlo simulations the PDB IDs 2ZT9 [15] and 4GYD (this work) were used for Cf and Cc6, respectively. The structure preparation and the Monte Carlo simulation [60] was similarly performed as was done before [40,61]. The iron of Cf and Cc6 were considered to be in the oxidized state. In order to match the experimental conditions, the electrostatic potential was calculated for an ionic strength of 0.01 M and a temperature of 298 K with APBS [62]. 10,000 randomly chosen encounters of the simulation were used for the analysis.

3. Results

3.1. Self-reduction of Cc6 and ligand mutagenesis

For the characterization of the complex of Cf and Cc6, paramagnetic relaxation enhancement (PRE) was used. With this method intermolecular PREs of Cc6 nuclei are measured that are caused by spin labels attached to the surface of Cf at various positions. The PREs are then converted into distance restraints for docking calculations. The spin label MTSL is linked to site-specific Cys residues engineered on Cf *via* a disulphide bridge. To maintain the spin label in the paramagnetic state and the disulphide bridge intact, it is essential that both cytochromes remain in the oxidized, ferric state. In the past we experienced rapid self-reduction with *c*-type cytochromes, a phenomenon that has been described also by others for yeast iso-1-cytochrome *c* [63]. To avoid the problem, it was decided to use a mutant Cc6 with a much lower redox potential to prevent self-reduction. Two mutants were produced in which the purposed axial Met ligand (M58) to the haem iron was replaced with either His or Cys.

The midpoint potential of wt Cc6 is 335 mV at pH 7.0 [38]. Both mutations result in a very large decrease of the midpoint potential, with $E_m = -140$ mV (pH 7.0) and −235 mV (pH 6.5) [25] for M58H and M58C Cc6, respectively. Thus, the replacement of the Met with a Cys ligand decreases the potential by 570 mV. To determine the effect of the mutation on the structure, the crystal structures were determined. Table 1 reports the refinement statistics and Fig. 1A illustrates the quality of the data. The structure of the wt Cc6 of *Nostoc* sp. PCC 7119 consists of the classic Cc fold, with 4 α-helices and 3 coils. The haem group is attached covalently to Cys14 and Cys17, and His18 and Met58 coordinate the iron. The structure is very similar to Cc6 from other sources, including green algae [18–22]. The closest resemblance is to Cc6 from *Phormidium laminosum* with an RMSD for the backbone heavy atoms of 0.58 Å (PDB ID: 2V08) [20]. The structures of the mutants are similar to that of the wt Cc6, with backbone RMSDs of 0.95 and 0.13 Å for M58H and M58C, respectively. Clearly, the M58C Cc6 structure is essentially identical to that of the wild type, although the thiolate–iron distance in M58C is longer for all six of the Cc6 molecules in the asymmetric unit (the average distance is 3.27 ± 0.04 Å) than the distance between the iron and the S^{δ} of the Met ligand (2.38 ± 0.06 Å). A picture of the electron density in this region for one of the molecules in shown in Fig. 1A.

Significant differences are observed for M58H Cc6 (Fig. 1, panels B and C). The His 58 N^{ε} is coordinated to the iron (2.02 Å), resulting in a backbone change around Lys 55, rotating it to a more solvent-exposed

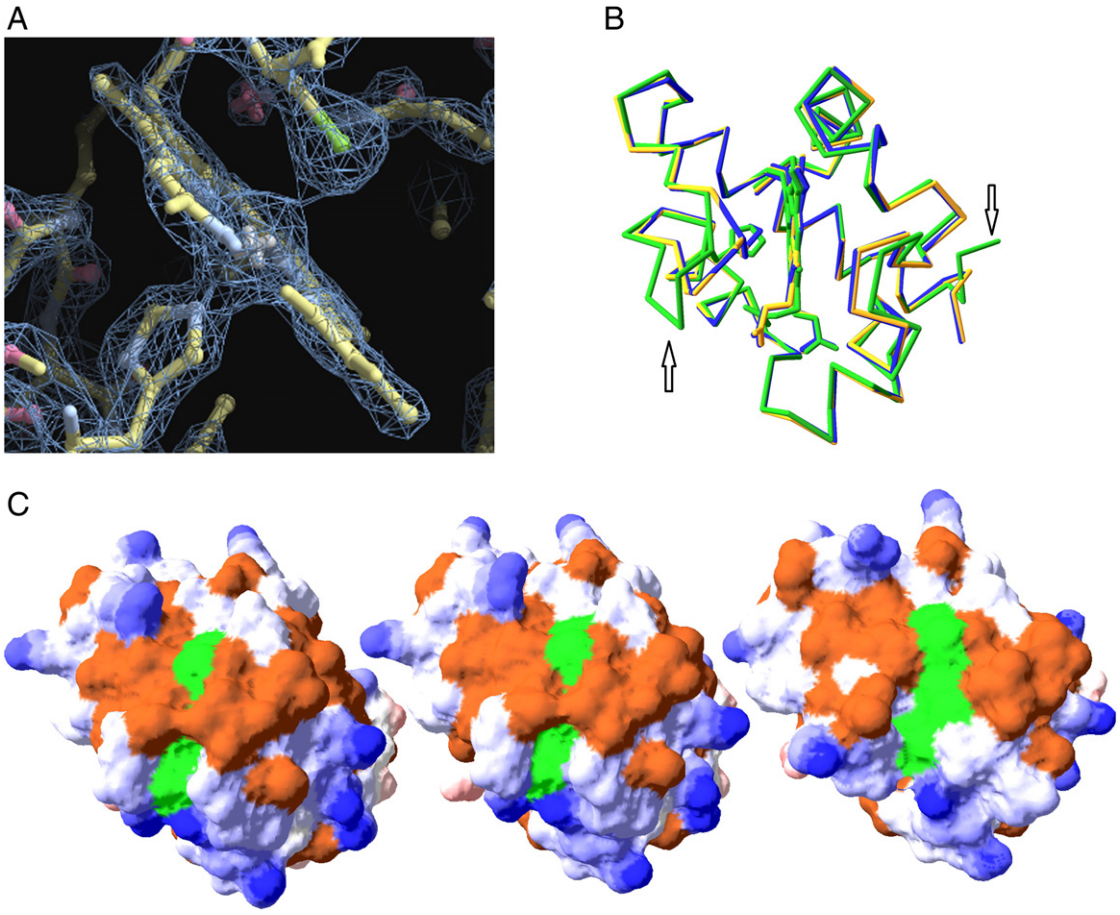

Fig. 1. Comparison of Cc6 structures. A) Electron density contoured at 2.2 sigma with the final M58C Cc6 model in the region around the haem iron. This figure was created with COOT [1]. B) Overlay of Cα traces of wt (blue), M58C (yellow) and M58H (green). Residue 58 and the haem are shown in sticks. The arrows indicate the large differences between M58H and wt Cc6. C) Surface representations of M58C (left), wt (middle) and M58H (right). The surface is coloured according to the surface potential from red to blue (negative to positive, calculated with DeepView (http://www.genebee.msu.su/spdbv). Non-polar residues are in brown and the haem is in green.

orientation. Surprisingly, also Trp85 and the C-terminal residue Lys86, on the other side of the protein, far from the His58, show a large displacement compared to the wt structure.

It was decided to use M58C Cc6 as a redox inactive substitute for the wt protein, because of its low midpoint potential and structural similarity. M58C Cc6 was enriched in ^{15}N and the amide nuclei were assigned on the basis of NOESY-^{15}N HSQC (150 ms mixing time) and TOCSY-^{15}N HSQC spectra with 80 ms mixing. For the M58C Cc6 variant, no self-reduction was observed, as expected from its low midpoint potential. The backbone amide assignments are reported in Table S1 in the supplementary information. Those corresponding to the two loops surrounding the haem edge are partly missing or tentative. Sequential connections were difficult to make in these regions, most likely due to some dynamics on the micro-millisecond timescale.

3.2. Dissociation constant and chemical shift map

To determine the affinity between M58C Cc6 and Cf a titration was performed. Ferrous Cf was titrated into M58C Cc6 and HSQC spectra were recorded at every point. Fig. 2, panel A shows the chemical-shift perturbations of several Cc6 amide nuclei plotted as a function of the Cf–Cc6 ratio. The curves can be fitted with a 1:1 binding model, yielding a binding constant of 7(2) mM^{-1}, identical within error to that for the wt complex, 8(2) mM^{-1} [34]. Panel B in Fig. 2 shows the binding map, in which the surface of the protein has been coloured according to the size of the average amide chemical-shift perturbation for each residue, extrapolated to the 100% bound state of Cc6 ($\Delta\delta_{Avg}$). The map is similar to the one reported for wt Cc6 binding to *Nostoc* [34] as well as *P. laminosum* Cf [33] and shows that the complex uses mainly the haem edge region for binding, although some residues at the other sides of the protein are affected, most notably Glu 68. The overall size of the shifts and this distribution of residues on the surface suggest that Cc6 mostly binds with one side toward Cf, in a relatively well-defined orientation [64]. Whether it binds on a single site of Cf cannot be established on the basis of these data.

3.3. Paramagnetic relaxation enhancements

To obtain intermolecular PREs for docking and structure determination of the complex, five mutants of Cf were produced in which cysteine residues were introduced on the surface of Cf in the region surrounding the haem. To avoid changes in the p*I*, which could affect the protein–protein interactions, only neutral amino acid residues were selected, Gln7, Ala63, Asn71, Gln104 and Ser192. Either the paramagnetic spin label MTSL or the non-paramagnetic analogue MTS was linked to the Cys residues. By measuring the intensity ratio of Cc6 M58C amide resonances in spectra recorded on samples with MTSL-Cf and MTS-Cf, the PRE was determined [56]. All the spin labels have large effects on Cc6 signals (Fig. S1). Interestingly, the effects are all found in the same region of Cc6, the loops centred around residues 20 and 55, which is also the area exhibiting the largest chemical-shift perturbations (Fig. 2). This observation suggests that Cc6 is always oriented toward Cf with this surface patch, comprising the region where the haem penetrates the surface, the haem edge. It also implies that Cc6 samples a significant surface area of Cf with this patch, because it is affected by the

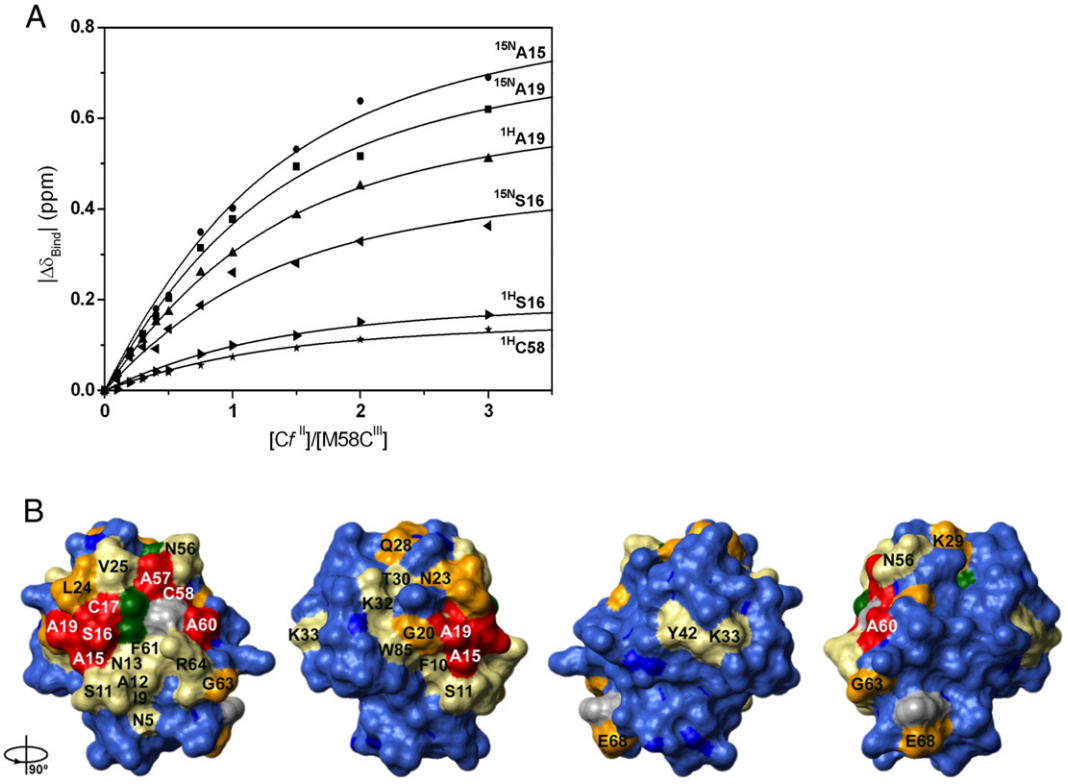

Fig. 2. Binding of M58C Cc6 to Cf. A) Binding curves for the interaction of M58C mutant with ferrous Cf. The data were fitted globally to a 1:1 model (non-linear, least-squares), yielding an association constant of 7 (±2) 10^3 M^{-1}. B) Chemical shift perturbation map. Residues for which a $\Delta\delta_{Avg}$ (ppm) was calculated are colour-coded on the structure of M58C mutant according to the following categories: blue for <0.025 ppm, yellow for ≥0.025 ppm, orange for ≥0.050 ppm, red for ≥0.125 ppm. Prolines are shown in grey and the haem group in dark green. Residues are identified with the single-letter amino acid code, and the surfaces have been rotated in anti-clockwise 90° steps around the vertical axis, with respect to the one on the left. Surface representations were generated using MOLMOL [2].

spin labels at every position. If it would assume a single orientation on Cf, located between the spin label positions, PREs from each spin label would affect a different side of Cc6.

3.4. Docking Cc6 in a single orientation

The PREs were converted into distances and docking calculations were performed. The spin label dynamics were represented by using four orientations per spin label [58] and the spin labels were allowed to rotate during the docking to avoid steric clashes with Cc6. The proteins were treated as rigid bodies. It turned out that Cc6 docks so closely to the spin labels (see below) that tiny distance variations led to very large changes in PRE, a consequence of dependence of the PRE on the sixth power of the distance between nucleus and spin label. For this reason it was preferable to use the PRE-based distances and not the PREs themselves as restraints in the docking calculations and evaluation of the quality of the fit with the observed data.

First, a simple model of Cc6 and Cf interaction was tested, by assuming that the PREs represent only a single, well-defined orientation of the proteins within the complex. The resultant structure that best fits the experimental data is physically unrealistic, because Cc6 does not make contact with Cf, but rather remains at a distance of several Ångström from the surface. The degree to which the structure represents the experimental data was expressed as the average distance violation, which represents the difference between the experimental and the back-calculated distances for all residues and all spin labels (the definition is given in the Materials and methods section). Thus, the larger the average violation, the poorer the quality of the fit. Fig. 3A shows that the average distance violation for the simple model, with a fraction of a well-defined structure of 100% (p = 0), is 2.0 Å. Figs. 4A and S2 plot the experimental and back-calculated distances for each residue. Several regions of Cc6 experience more paramagnetic effects than predicted by this model and these residues are expected to be closer to the spin label than is found in the model. It is clear that the PRE data cannot be described by Cc6 in a single orientation within the complex with Cf.

3.5. Ensemble docking

Ensemble docking was used to obtain a better fit to the experimental data. This approach assumes that the complex exists in more than a

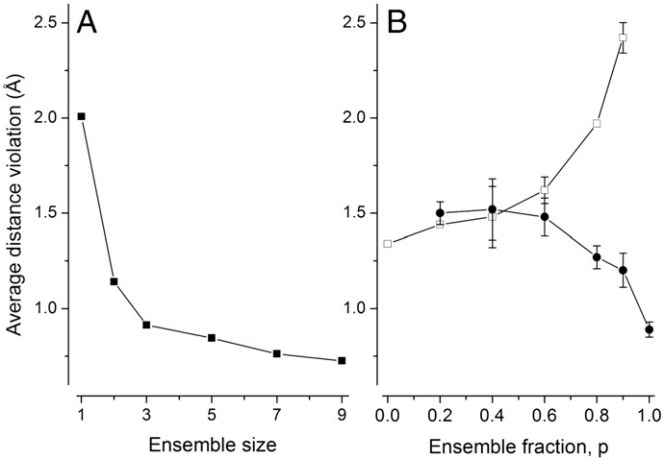

Fig. 3. Average violation plots. A) The average distance violation plotted for increasing ensemble size. B) The average distance violation is plotted for different ensemble fractions (p). The results for the average violation for the single structure only (open symbols) and for the combination of single structure and ensemble (solid symbols) are shown. For p = 1, the complex consists entirely of an ensemble. The ensemble size used in these calculations was five. The definition of the error bars is given in the Materials and methods section.

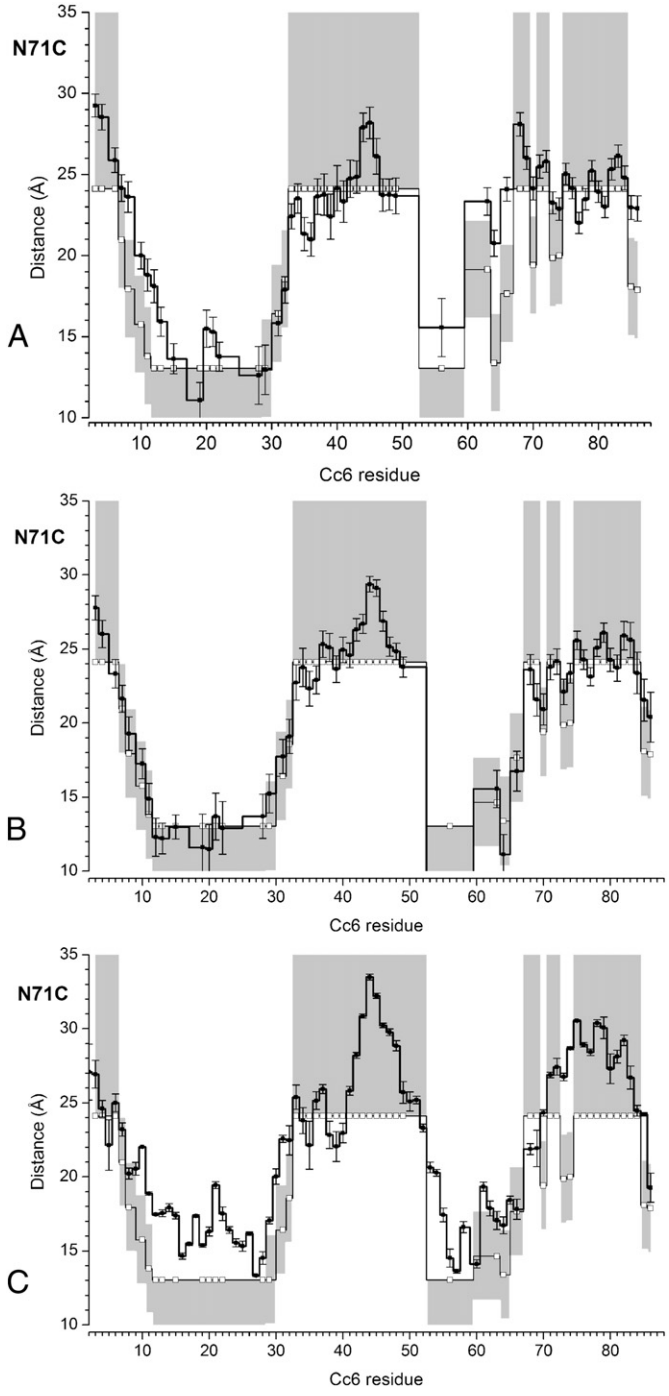

Fig. 4. Fitting of the experimental distances. The average distances between the oxygen atom of spin label N71C and Cc6 amide protons were back-calculated from various ensembles (thick line and solid symbols), plotted against the residue number and compared with the experimental distances (open symbols). The grey areas indicate the experimental error margins. In (A, B) the solid line represents the averages for the ten best structures obtained from docking a single copy (A), or ten ensembles of five copies (B) of Cc6. In (C), it represents the averages from three sets of 10,000 randomly selected structures from the MC ensemble. The error bars indicate the SD of the ensembles.

single orientation and can be represented by an ensemble of orientations [65]. Several copies of Cc6 were docked simultaneously, driven by the PRE-derived distances. The average distance between the spin label and the set of identical nuclei in the ensemble was compared with the experimental distance and minimized, resulting in an ensemble of orientations of Cc6 around Cf. This procedure was repeated many times, creating a cloud of orientations. The quality of the fit is expressed as the average violation of the experimental distances. The size of the ensemble, which is the number of copies of Cc6 used in the docking, was varied, demonstrating that the fit improvement by adding more copies levels off quickly (Fig. 3A). In the subsequent calculations an ensemble size of five Cc6 copies was used. Adding more copies does not significantly improve the fits and results in superfluous copies of Cc6 that are placed far from the surface of Cf.

The ensemble docking can be executed assuming that all the PREs derive from this ensemble (100% ensemble, $p = 1$) or that a two-state model is applicable, with a dynamic encounter state and a well-defined state ($0 < p < 1$). In the latter case, a single Cc6 molecule is docked first, assuming a certain population, for example 40%, and then the back-calculated PRE effects for this structure are subtracted from the observed PREs and the remaining PREs are input for the subsequent ensemble docking to obtain the encounter complex that represents the remaining 60% of the complex [66]. The back-calculated distances from the combined single structure + ensemble are compared with the experimental distances to evaluate the quality of the fit. Fig. 3B shows the results for such calculations. The average distance violation is plotted as a function of the fraction of encounter complex (p), for the single structures only (open symbols) and for the single structure + ensemble, representing the entire complex (solid symbols). As expected, ensemble docking yields lower average violations, because more degrees of freedom are added in such calculations. Interestingly, the fit does not improve for p-values up to 0.6. That means that a large fraction of the PRE is attributable to the encounter complex. The best results are found for $p = 1.0$, so in the absence of a single, well-defined orientation of Cc6. These results suggest that a single dominant orientation is not present and that the complex of Cf and Cc6 is best described by an ensemble of orientations.

The average distances back-predicted from the ensemble ($p = 1.0$) fit the experimental distance much better than the single structure (Figs. 4B and S3), indicating that the ensemble is an acceptable representation of the PRE data.

3.6. Monte Carlo docking calculations

We then wondered whether the ensemble is of purely electrostatic nature. Before, it had been shown that the encounter complex of cytochrome *c* peroxidase and cytochrome *c* could be described by a theoretical ensemble obtained *via* Monte Carlo (MC) calculations that only considered electrostatic interactions between the proteins [61]. Similar calculations were performed for the Cf–Cc6 complex and a large ensemble was created. From this ensemble the average distances from the Cc6 amide protons and the spin labels were calculated and compared with the experimental distances (Figs. 4C and S4). The distance patterns roughly follow the experimental ones, but it is clear that the MC ensemble cannot describe the experimental data very well. In most of the MC orientations Cc6 is oriented with its haem edge face oriented toward the Cf surface, in line with the conclusion from the experimental PRE patterns. Thus, it can be concluded that Cc6 pre-orients this face toward Cf upon its approach, due to electrostatic interactions. However, the poor quantitative match with the experimental distances indicates that the places where Cc6 is located on the Cf surface in the MC ensemble do not agree well with the real complex, suggesting that within the encounter complex, other interactions than electrostatics contribute significantly.

3.7. Analysis of the ensemble

The centres-of-mass of the 610 Cc6 molecules obtained from 122 runs of ensemble docking show that Cc6 visits an area including and surrounding the hydrophobic surface patch near the haem of Cf (Fig. 5, green). Clearly, a single structure cannot describe this ensemble. It is possible that the Cc6 samples an even larger area, because the five spin labels did not cover the whole surface of Cf, so in the calculations

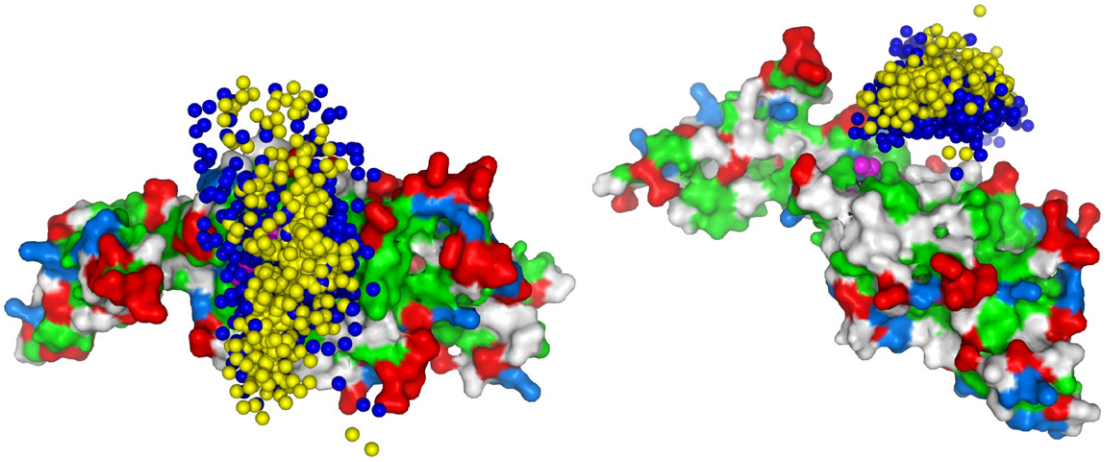

Fig. 5. The ensemble of Cc6 around Cf shown in two orientations. Cf is shown in surface representation with the haem in magenta spheres. Negative, positive and hydrophobic residues (including Tyr and Trp) of Cf are displayed in red, marine and green, respectively. The yellow and dark blue spheres represent the centres-of-mass and iron atoms of Cc6 in the ensemble, respectively.

there are no restraints to guide Cc6 to those regions. The charge distribution on Cf shows that it has an overall negative charge, with strong negative potential around the hydrophobic patch. Cc6 has a ring of positive charges around its hydrophobic patch, close to the haem edge (Fig. 1C). Cc6 is always oriented with this region toward Cf, as can be seen in Fig. 5. The blue spheres represent the iron atoms of Cc6 in the ensemble. These atoms are always closer to Cf than the centres-of-mass (yellow spheres), indicating that Cc6 has a preferred binding orientation. Most of the Cc6 molecules are found to interact with the hydrophobic patch of Cf, not with the charged regions, in accord with the finding that the MC calculations, which are based purely on charge–charge interactions, do not produce an ensemble that fits the experimental data well.

4. Discussion

Characterization of the complex of Cf and Cc6 was hindered by self-reduction of Cc6 during NMR experiments. A solution was found by replacement of the methionine ligand of the haem iron. Substitution with a His or a Cys residue resulted in a large decrease of the midpoint potential. The crystal structures of the *Nostoc* wt Cc6 and both variants were determined. In particular the Cys mutant is remarkably similar in structure to the wt protein, despite the shorter side chain length of Cys. Mutant M58C was used in the interactions studies with Cf, because its low midpoint potential abolished the problem of self-reduction. Substitution of haem ligands by Cys has been reported for haem enzymes to study the effects on enzyme activity ([67] and references therein) and the spectroscopic characterization of semi-synthetic Cc with a Cys replacing the ligand Met has been described [68,69]. Very recently, an extensive study of yeast Cc with a co-ordinating Cys was published. Replacement of the Thr at position 78 by Cys yielded a protein that was more stable than Met80Cys Cc [70]. It is difficult to produce redox-inactive cytochrome *c* analogues by metal substitution, because removal of the haem iron can only be achieved under harsh conditions, requiring denaturation and refolding of the protein. The substitution of Met co-ordination by that with a Cys thiolate can be used as a convenient alternative. In each of the described cases the midpoint potentials dropped by many hundreds of mV.

The PRE data indicate that the complex is not dominated by a single well-defined orientation, but instead it is best described by an ensemble of orientations. The chemical-shift perturbation results as well as the PRE data indicate that Cc6 pre-orients upon approaching Cf. It is expected that the long-range electrostatic attraction causes Cc6 to orient with its positive charges toward the overall negative Cf. Given the dipolar nature of Cc6, this movement results in Cc6 facing Cf with its hydrophobic patch located around the haem edge. It has been known for a long time that the haem edge provides strong coupling for electron transfer, so the pre-orientation primes Cc6 for rapid electron transfer from the Cf haem. At a short distance, hydrophobic interactions appear to be important, because the ensemble that fits the PRE data is located mostly above the hydrophobic region around the Cf haem group. Contrary to the encounter complex of the electron transfer complex of cytochrome *c* and cytochrome *c* peroxidase, which can be described with electrostatic interactions only [57,61], the Cf–Cc6 complex also involves hydrophobic interactions. These findings are in line with recent studies on the Cf–Pc complex from the same *Nostoc* species [40,41]. Also in that case the complex is at least partly in an encounter state and electrostatic MC calculations cannot fully describe the PRE data. In this complex hydrophobic interactions appear to play a similarly important role, which became clear from a recent comparative study on Cf–Pc complexes from *Nostoc* and *P. laminosum* [71]. Other studies on Cc6 from *Nostoc* and *C. reinhardtii*, using NMR, kinetic measurements and docking calculations also indicated the importance of hydrophobic interactions with its partners, Cf [31–33], photosystem I [26,29] and cytochrome *c* oxidase [72]. The data further suggest that the Cf–Cc6 complex consists predominantly or entirely of an ensemble of orientations, whereas in the Cf–Pc complex a stereospecific complex is also present for a significant amount of the time.

These studies raise the question whether the two state model of an electrostatic encounter complex and a well-defined complex, with specific hydrophobic interactions, hydrogen bonding and van der Waals forces as well as electrostatic interactions, is generally applicable to electron transfer complexes. At least in the *Nostoc* case, of Cf reacting with Cc6 and Pc, the complex is better described by electrostatic pre-orientation when the proteins are still approaching and an ensemble of orientations in which the proteins exhibit a form of hydrophobic sliding, with increasing desolvation of the hydrophobic patches and thus a gradual transition to the most stably bound orientation (Cf–Pc) or orientations (Cf–Cc6) [40]. The model is illustrated in Fig. 6. Such a hydrophobic search mechanism has been suggested on the basis of theoretical studies by Camacho and co-workers [73,74]. Although the encounter complex is normally considered to be dominated by electrostatic interactions [3,75,76], the involvement of hydrophobic contacts in the encounter state has been reported before [40,66,71,77].

In the ensemble some orientations will exhibit optimal coupling between the redox centres, resulting in rapid electron transfer. As long as the distance between the haems is short and the space jump between the proteins is small, electron transfer will be fast. A single, well-defined orientation is not required in that case. In fact, it is not desirable, because a well-defined complex needs to be stabilized by multiple

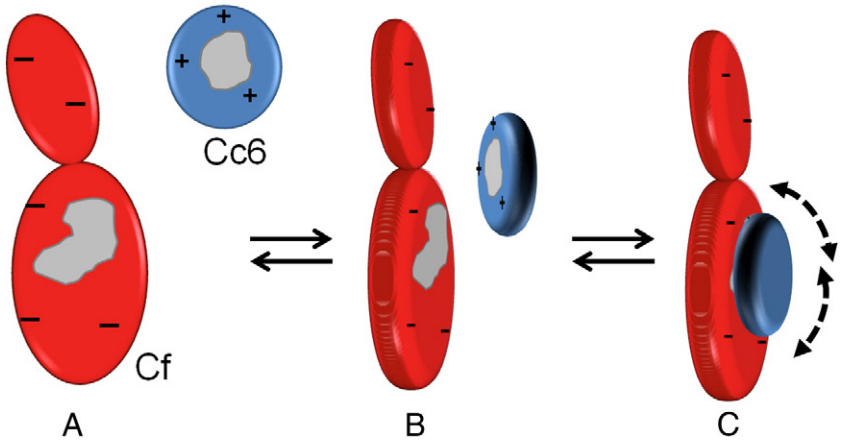

Fig. 6. Model for complex formation of Cf and Cc6. A) Free proteins approach *via* diffusion. B) Electrostatic pre-orientation during approach. C) Cc6 slides over the surface of Cf optimizing hydrophobic contacts (grey areas). Some of the positions in this state are compatible with fast electron transfer.

interactions, making it too stable for rapid dissociation. The view that in some complexes multiple orientations, part of a larger ensemble, are suited for ET, is similar to the dynamic docking model described for myoglobin and cytochrome b_5, although that complex appears to be dominated by charge–charge interactions [78,79]. It is supported by a recently published kinetic study demonstrating that multiple conformations of Cc6 contribute to electron transfer within the Cf–Cc6 complex [31]. In the described model of gradual desolvation, the reverse process happens upon dissociation. Gradual resolvation avoids a high transition state barrier between the electron transfer active state and the free proteins, thus ensuring rapid dissociation. For photosynthetic electron transfer proteins, a high off-rate is as important as fast electron transfer to avoid product inhibition and reduction of the electron flow rate in the redox chain [80]. The relatively low affinity between Cf and its partners is in line with the idea that rapid turn-over is important. In the thylakoids, Cf is present in a tilted orientation, with the side shown in Fig. 5 facing the lumen. The other side is close to the membrane and not accessible to Cc6 and Pc. Given the considerable confinement within the lumen, it is expected that the local concentrations are high and affinity is not a stringent requirement for complex formation.

5. Conclusions

The findings on the complexes of Cf with Pc and Cc6 show that encounter complexes represent an important part of the photosynthetic ET protein complexes. Experimental evidence for a role of hydrophobic interactions in the encounter complex is accumulating, blurring the distinction between encounter complex and stereospecific complex. This is true in particular for ET complexes, because a distance between the metal ions that is sufficiently short for rapid ET is all that is required for activity, so there is no reason for the presence of a single active orientation within the complex.

Acknowledgements

We thank Daniel de Geus, Ellen Thomassen and Irakli Sikharulidze for assistance in the X-ray diffraction data collection. Financial support was provided by the Netherlands Organisation for Scientific Research (NWO), through VIDI Grant Nos. 700.52.425 (RH, MU) and 700.55.425 (NSP), VICI Grant No. 700.58.441 (MU), and Open Competition Grant No. 700.50.026 (MF), by the Spanish Ministry of Economy and Competiveness (Grant Nos. BFU2003-00458/BMC, BFU2006-01361/BMC, BFU2009-07190/BMC and BFU2012-31670/BMC) and by the Andalusian Government (Grant PAI, BIO198). IDM was supported by the Human Potential Programme and the Mobility of Researchers Programme of the European Commission (Contract No. HPRN-CT-1999-00095) and by the Ministry of Education, Culture and Sports, Spain (Grant No. AP2000-2937). BMB was awarded with a PhD fellowship (AP2009-4092) from the Ministry of Education, Culture and Sports, Spain, co-funded by the European Social Fund, ERDF (2007–2013). DC and GLR were supported by the Italian Ministry of University and Research, MIUR (Grant PRIN 20074TJ3ZB_004). JMF and GMU were supported by Grant DFG RTG 1640 of the Deutsche Forschungsgemeinschaft.

Appendix A. Supplementary data

Supplementary data include a table with assignments of Cc6 amides, intensity ratio plots (I_{para}/I_{dia}), distance plots for single structure and ensemble docking and Monte-Carlo simulations, an example of an ensemble docking script for XPLOR and an input file with PRE restraints.

Deposits

PDB IDs: Cc6 wt (4GYD), M58C (4H0J) and M58H (4H0K). Supplementary data to this article can be found online at DOI: http://dx.doi.org/10.1016/j.bbabio.2014.03.009.

References

[1] P. Emsley, B. Lohkamp, W.G. Scott, K. Cowtan, Features and development of Coot, Acta Crystallogr. D 66 (2010) 486–501.
[2] R. Koradi, M. Billeter, K. Wuthrich, MOLMOL: a program for display and analysis of macromolecular structures, J. Mol. Graph. 14 (1996) 51–55.
[3] M. Ubbink, The courtship of proteins: understanding the encounter complex, FEBS Lett. 583 (2009) 1060–1066.
[4] C.C. Moser, J.M. Keske, K. Warncke, R.S. Farid, P.L. Dutton, Nature of biological electron transfer, Nature 355 (1992) 796–802.
[5] A. Diaz-Quintana, J.A. Navarro, M. Hervás, F.P. Molina-Heredia, B. De la Cerda, M.A. De la Rosa, A comparative structural and functional analysis of cyanobacterial plastocyanin and cytochrome c(6) as alternative electron donors to Photosystem I — Photosystem I reduction in cyanobacteria, Photosynth. Res. 75 (2003) 97–110.
[6] B. De la Cerda, J.A. Navarro, M. Hervás, M.A. De la Rosa, Changes in the reaction mechanism of electron transfer from plastocyanin to photosystem I in the cyanobacterium *Synechocystis* sp. PCC 6803 as induced by site-directed mutagenesis of the copper protein, Biochemistry 36 (1997) 10125–10130.
[7] J. Sun, W. Xu, M. Hervás, J.K. Navarro, M.A. De la Rosa, P.R. Chitnis, Oxidizing side of the cyanobacterial photosystem I — evidence for interaction between the electron donor proteins and a luminal surface helix of the PsaB subunit, J. Biol. Chem. 274 (1999) 19048–19054.
[8] G.M. Ullmann, M. Hauswald, A. Jensen, N.M. Kostic, E.W. Knapp, Comparison of the physiologically equivalent proteins cytochrome c6 and plastocyanin on the basis of their electrostatic potentials. Tryptophan 63 in cytochrome c6 may be isofunctional with tyrosine 83 in plastocyanin, Biochemistry 36 (1997) 16187–16196.
[9] R.V. Duran, M. Hervás, M.A. De la Rosa, J.A. Navarro, The efficient functioning of photosynthesis and respiration in *Synechocystis* sp PCC 6803 strictly requires the presence of either cytochrome c_6 or plastocyanin, J. Biol. Chem. 279 (2004) 7229–7233.
[10] M.A. De la Rosa, J.A. Navarro, A. Diaz-Quintana, B. De la Cerda, F.P. Molina-Heredia, A. Balme, P.D. Murdoch, I. Diaz-Moreno, R.V. Duran, M. Hervás, An evolutionary analysis of the reaction mechanisms of photosystem I reduction by cytochrome c(6) and plastocyanin, Bioelectrochemistry 55 (2002) 41–45.
[11] R. Gupta, Z.Y. He, S. Luan, Functional relationship of cytochrome c(6) and plastocyanin in *Arabidopsis*, Nature 417 (2002) 567–571.

[12] F.P. Molina-Heredia, J. Wastl, J.A. Navarro, D.S. Bendall, M. Hervás, C.J. Howe, M.A. De la Rosa, A new function for an old cytochrome? Nature 424 (2003) 33–34.
[13] D. Stroebel, Y. Choquet, J.L. Popot, D. Picot, An atypical haem in the cytochrome b(6)f complex, Nature 426 (2003) 413–418.
[14] G. Kurisu, H.M. Zhang, J.L. Smith, W.A. Cramer, Structure of the cytochrome b_6f complex of oxygenic photosynthesis: tuning the cavity, Science 302 (2003) 1009–1014.
[15] D. Baniulis, E. Yamashita, J.P. Whitelegge, A.I. Zatsman, M.P. Hendrich, S.S. Hasan, C. M. Ryan, W.A. Cramer, Structure–function, stability, and chemical modification of the cyanobacterial cytochrome b(6)f complex from *Nostoc* sp. PCC 7120, J. Biol. Chem. 284 (2009) 9861–9869.
[16] S.E. Martinez, D. Huang, A. Szczepaniak, W.A. Cramer, J.L. Smith, Crystal-structure of chloroplast cytochrome *f* reveals a novel cytochrome fold and unexpected heme ligation, Structure 2 (1994) 95–105.
[17] I. Diaz-Moreno, S. Diaz-Moreno, G. Subias, M.A. De la Rosa, A. Diaz-Quintana, The atypical iron-coordination geometry of cytochrome *f* remains unchanged upon binding to plastocyanin, as inferred by XAS, Photosynth. Res. 90 (2006) 23–28.
[18] M. Beissinger, H. Sticht, M. Sutter, A. Ejchart, W. Haehnel, P. Rosch, Solution structure of cytochrome c(6) from the thermophilic cyanobacterium *Synechococcus elongatus*, EMBO J. 17 (1998) 27–36.
[19] M.R. Sawaya, D.W. Krogmann, A. Serag, K.K. Ho, T.O. Yeates, C.A. Kerfeld, Structures of cytochrome *c*-549 and cytochrome *c*(6) from the cyanobacterium *Arthrospira maxima*, Biochemistry 40 (2001) 9215–9225.
[20] J.A.R. Worrall, B.G. Schlarb-Ridley, T. Reda, M.J. Marcaida, R.J. Moorlen, J. Wastl, J. Hirst, D.S. Bendall, B.F. Luisi, C.J. Howe, Modulation of heme redox potential in the cytochrome *c*(6) family, J. Am. Chem. Soc. 129 (2007) 9468–9475.
[21] W. Bialek, S. Krzywda, M. Jaskolski, A. Szczepaniak, Atomic-resolution structure of reduced cyanobacterial cytochrome *c*(6) with an unusual sequence insertion, FEBS J. 276 (2009) 4426–4436.
[22] L. Banci, I. Bertini, M.A. De la Rosa, D. Koulougliotis, J.A. Navarro, O. Walter, Solution structure of oxidized cytochrome *c*(6) from the green alga *Monoraphidium braunii*, Biochemistry 37 (1998) 4831–4843.
[23] M.J. Marcaida, B.G. Schlarb-Ridley, J.A.R. Worrall, J. Wastl, T.J. Evans, D.S. Bendall, B.F. Luisi, C.J. Howe, Structure of cytochrome *c*(6A), a novel dithio-cytochrome of *Arabidopsis thaliana*, and its reactivity with plastocyanin: implications for function, J. Mol. Biol. 360 (2006) 968–977.
[24] B.S. Rajagopal, M.T. Wilson, D.S. Bendall, C.J. Howe, J.A.R. Worrall, Structural and kinetic studies of imidazole binding to two members of the cytochrome *c*(6) family reveal an important role for a conserved heme pocket residue, J. Biol. Inorg. Chem. 16 (2011) 577–588.
[25] A. Kranich, H. Naumann, F.P. Molina-Heredia, H.J. Moore, T.R. Lee, S. Lecomte, M.A. De la Rosa, P. Hildebrandt, D.H. Murgida, Gated electron transfer of cytochrome *c*(6) at biomimetic interfaces: a time-resolved SERR study, Phys. Chem. Chem. Phys. 11 (2009) 7390–7397.
[26] I. Diaz-Moreno, A. Diaz-Quintana, F.P. Molina-Heredia, P.M. Nieto, O. Hansson, M.A. De la Rosa, B.G. Karlsson, NMR analysis of the transient complex between membrane photosystem I and soluble cytochrome *c*(6), J. Biol. Chem. 280 (2005) 7925–7931.
[27] I. Diaz-Moreno, A. Diaz-Quintana, G. Subias, T. Mairs, M.A. De la Rosa, S. Diaz-Moreno, Detecting transient protein–protein interactions by X-ray absorption spectroscopy: the cytochrome *c*(6)–photosystem I complex, FEBS Lett. 580 (2006) 3023–3028.
[28] M. Hervás, J.A. Navarro, M.A. De la Rosa, Electron transfer between membrane complexes and soluble proteins in photosynthesis, Acc. Chem. Res. 36 (2003) 798–805.
[29] F.P. Molina-Heredia, A. Diaz-Quintana, M. Hervás, J.A. Navarro, M.A. De la Rosa, Site-directed mutagenesis of cytochrome *c*(6) from *Anabaena* species PCC 7119 — identification of surface residues of the hemeprotein involved in photosystem I reduction, J. Biol. Chem. 274 (1999) 33565–33570.
[30] F.P. Molina-Heredia, M. Hervás, J.A. Navarro, M.A. De la Rosa, A single arginyl residue in plastocyanin and in cytochrome *c*(6) from the cyanobacterium *Anabaena* sp. PCC 7119 is required for efficient reduction of photosystem I, J. Biol. Chem. 276 (2001) 601–605.
[31] T.Z. Grove, G.M. Ullmann, N.M. Kostic, Simultaneous true, gated, and coupled electron-transfer reactions and energetics of protein rearrangement, J. Inorg. Biochem. 106 (2012) 143–150.
[32] T.Z. Grove, N.M. Kostic, Metalloprotein association, self-association, and dynamics governed by hydrophobic interactions: simultaneous occurrence of gated and true electron-transfer reactions between cytochrome *f* and cytochrome c_6 from *Chlamydomonas reinhardtii*, J. Am. Chem. Soc. 125 (2003) 10598–10607.
[33] P.B. Crowley, A. Diaz-Quintana, F.P. Molina-Heredia, P. Nieto, M. Sutter, W. Haehnel, M.A. De la Rosa, M. Ubbink, The interactions of cyanobacterial cytochrome c_6 and cytochrome *f*, characterized by NMR, J. Biol. Chem. 277 (2002) 48685–48689.
[34] I. Diaz-Moreno, A. Diaz-Quintana, M. Ubbink, M.A. De la Rosa, An NMR-based docking model for the physiological transient complex between cytochrome *f* and cytochrome *c*(6), FEBS Lett. 579 (2005) 2891–2896.
[35] E.L. Gross, D.C. Pearson, Brownian dynamics. Simulations of the interaction of *Chlamydomonas* cytochrome *f* with plastocyanin and cytochrome c_6, Biophys. J. 85 (2003) 2055–2068.
[36] E.J. Haddadian, E.L. Gross, Brownian dynamics study of cytochrome *f* interactions with cytochrome *c*(6) and plastocyanin in *Chlamydomonas reinhardtii* plastocyanin, and cytochrome *c*(6) mutants, Biophys. J. 88 (2005) 2323–2339.
[37] E.J. Haddadian, E.L. Gross, A Brownian dynamics study of the effects of cytochrome *f* structure and deletion of its small domain in interactions with cytochrome *c*(6) and plastocyanin in *Chlamydomonas reinhardtii*, Biophys. J. 90 (2006) 566–577.
[38] F.P. Molina-Heredia, M. Hervás, J.A. Navarro, M.A. De la Rosa, Cloning and correct expression in *Escherichia coli* of the petE and petJ genes respectively encoding plastocyanin and cytochrome c_6 from the cyanobacterium *Anabaena* sp. PCC 7119, Biochem. Biophys. Res. Commun. 243 (1998) 302–306.
[39] C. Albarran, J.A. Navarro, F.P. Molina-Heredia, P.S. Murdoch, M.A. De la Rosa, M. Hervas, Laser flash-induced kinetic analysis of cytochrome *f* oxidation by wild-type and mutant plastocyanin from the cyanobacterium *Nostoc* sp. PCC 7119, Biochemistry 44 (2005) 11601–11607.
[40] S. Scanu, J.M. Foerster, G.M. Ullmann, M. Ubbink, Role of hydrophobic interactions in the encounter complex formation of the plastocyanin and cytochrome *f* complex revealed by paramagnetic NMR spectroscopy, J. Am. Chem. Soc. 135 (2013) 7681–7692.
[41] S. Scanu, J. Förster, M.G. Finiguerra, M.H. Shabestari, M. Huber, M. Ubbink, The complex of cytochrome *f* and plastocyanin from *Nostoc* sp. PCC 7119 is highly dynamic, ChemBioChem 13 (2012) 1312–1318.
[42] E. Arslan, H. Schulz, R. Zufferey, P. Kunzler, L. Thony-Meyer, Overproduction of the *Bradyrhizobium japonicum* c-type cytochrome subunits of the cbb(3) oxidase in *Escherichia coli*, Biochem. Biophys. Res. Commun. 251 (1998) 744–747.
[43] A.G.W. Leslie, Integration of macromolecular diffraction data, Acta Crystallogr. D 55 (1999) 1696–1702.
[44] P. Evans, Scaling and assessment of data quality, Acta Crystallogr. D 62 (2006) 72–82.
[45] M.D. Winn, C.C. Ballard, K.D. Cowtan, E.J. Dodson, P. Emsley, P.R. Evans, R.M. Keegan, E.B. Krissinel, A.G.W. Leslie, A. Mccoy, S.J. McNicholas, G.N. Murshudov, N.S. Pannu, E.A. Potterton, H.R. Powell, R.J. Read, A. Vagin, K.S. Wilson, Overview of the CCP4 suite and current developments, Acta Crystallogr. D 67 (2011) 235–242.
[46] N.S. Pannu, W.J. Waterreus, P. Skubak, I. Sikharulidze, J.P. Abrahams, R.A.G. de Graaff, Recent advances in the CRANK software suite for experimental phasing, Acta Crystallogr. D 67 (2011) 331–337.
[47] R.A.G. de Graaff, M. Hilge, J.L. van der Plas, J.P. Abrahams, Matrix methods for solving protein substructures of chlorine and sulfur from anomalous data, Acta Crystallogr. D 57 (2001) 1857–1862.
[48] K. Cowtan, Error estimation and bias correction in phase-improvement calculations, Acta Crystallogr. D 55 (1999) 1555–1567.
[49] A. Perrakis, R. Morris, V.S. Lamzin, Automated protein model building combined with iterative structure refinement, Nat. Struct. Biol. 6 (1999) 458–463.
[50] P. Skubak, G.N. Murshudov, N.S. Pannu, Direct incorporation of experimental phase information in model refinement, Acta Crystallogr. D 60 (2004) 2196–2201.
[51] G.N. Murshudov, P. Skubak, A.A. Lebedev, N.S. Pannu, R.A. Steiner, R.A. Nicholls, M.D. Winn, F. Long, A.A. Vagin, REFMAC5 for the refinement of macromolecular crystal structures, Acta Crystallogr. D 67 (2011) 355–367.
[52] D.E. McRee, XtalView Xfit — a versatile program for manipulating atomic coordinates and electron density, J. Struct. Biol. 125 (1999) 156–165.
[53] P.J. Kraulis, Ansig — a program for the assignment of protein H-1 2D-NMR spectra by interactive computer-graphics, J. Magn. Reson. 84 (1989) 627–633.
[54] M. Helgstrand, P. Kraulis, P. Allard, T. Hard, Ansig for Windows: an interactive computer program for semiautomatic assignment of protein NMR spectra, J. Biomol. NMR 18 (2000) 329–336.
[55] A. Kannt, S. Young, D.S. Bendall, The role of acidic residues of plastocyanin in its interaction with cytochrome *f*, Biochim. Biophys. Acta Bioenerg. 1277 (1996) 115–126.
[56] J.L. Battiste, G. Wagner, Utilization of site-directed spin labeling and high-resolution heteronuclear nuclear magnetic resonance for global fold determination of large proteins with limited nuclear overhauser effect data, Biochemistry 39 (2000) 5355–5365.
[57] A.N. Volkov, J.A.R. Worrall, E. Holtzmann, M. Ubbink, Solution structure and dynamics of the complex between cytochrome *c* and cytochrome *c* peroxidase determined by paramagnetic NMR, Proc. Natl. Acad. Sci. U. S. A. 103 (2006) 18945–18950.
[58] J. Iwahara, C.D. Schwieters, G.M. Clore, Ensemble approach for NMR structure refinement against H-1 paramagnetic relaxation enhancement data arising from a flexible paramagnetic group attached to a macromolecule, J. Am. Chem. Soc. 126 (2004) 5879–5896.
[59] C.D. Schwieters, J.J. Kuszewski, N. Tjandra, G.M. Clore, The Xplor-NIH NMR molecular structure determination package, J. Magn. Reson. 160 (2003) 65–73.
[60] G.M. Ullmann, E.W. Knapp, N.M. Kostic, Computational simulation and analysis of dynamic association between plastocyanin and cytochrome *f*. Consequences for the electron-transfer reaction, J. Am. Chem. Soc. 119 (1997) 42–52.
[61] Q. Bashir, A.N. Volkov, G.M. Ullmann, M. Ubbink, Visualization of the encounter ensemble of the transient electron transfer complex of cytochrome *c* and cytochrome *c* peroxidase, J. Am. Chem. Soc. 132 (2010) 241–247.
[62] N.A. Baker, D. Sept, S. Joseph, M.J. Holst, J.A. McCammon, Electrostatics of nanosystems: application to microtubules and the ribosome, Proc. Natl. Acad. Sci. U. S. A. 98 (2001) 10037–10041.
[63] S.J. Moench, J.D. Satterlee, A comparison of spectral and physicochemical properties of yeast iso-1 cytochrome *c* and Cys 102-modified derivatives of the protein, J. Protein Chem. 14 (1995) 567–582.
[64] Q. Bashir, S. Scanu, M. Ubbink, Dynamics in electron transfer protein complexes, FEBS J. 278 (2011) 1391–1400.
[65] C. Tang, J. Iwahara, G.M. Clore, Visualization of transient encounter complexes in protein–protein association, Nature 444 (2006) 383–386.
[66] Y.C. Kim, C. Tang, G.M. Clore, G. Hummer, Replica exchange simulations of transient encounter complexes in protein–protein association, Proc. Natl. Acad. Sci. U. S. A. 105 (2008) 12855–12860.
[67] S.W. Vetter, A.C. Terentis, R.L. Osborne, J.H. Dawson, D.B. Goodin, Replacement of the axial histidine heme ligand with cysteine in nitrophorin 1: spectroscopic and crystallographic characterization, J. Biol. Inorg. Chem. 14 (2009) 179–191.
[68] A.L. Raphael, H.B. Gray, Semisynthesis of axial-ligand (position 80) mutants of cytochrome *c*, J. Am. Chem. Soc. 113 (1991) 1038–1040.

[69] C.J. Wallace, I. Clark-Lewis, Functional role of heme ligation in cytochrome *c*. Effects of replacement of methionine 80 with natural and non-natural residues by semisynthesis, J. Biol. Chem. 267 (1992) 3852–3861.
[70] F.F. Zhong, G.P. Lisi, D.P. Collins, J.H. Dawson, E.V. Pletneva, Redox-dependent stability, protonation, and reactivity of cysteine-bound heme proteins, Proc. Natl. Acad. Sci. U. S. A. 111 (2014) E306–E315.
[71] S. Scanu, J.M. Foerster, M. Timmer, G.M. Ullmann, M. Ubbink, Loss of electrostatic interactions causes increase of dynamics within the plastocyanin–cytochrome *f* complex, Biochemistry 52 (2013) 6615–6626.
[72] S.E. Hart, C.J. Howe, K. Mizuguchi, J. Fernandez-Recio, Docking of cytochrome *c*(6) and plastocyanin to the aa(3)-type cytochrome *c* oxidase in the cyanobacterium *Phormidium laminosum*, Protein Eng. Des. Sel. 21 (2008) 689–698.
[73] C.J. Camacho, S.R. Kimura, C. DeLisi, S. Vajda, Kinetics of desolvation-mediated protein–protein binding, Biophys. J. 78 (2000) 1094–1105.
[74] C.J. Camacho, Z.P. Weng, S. Vajda, C. DeLisi, Free energy landscapes of encounter complexes in protein–protein association, Biophys. J. 76 (1999) 1166–1178.
[75] G. Schreiber, G. Haran, H.X. Zhou, Fundamental aspects of protein–protein association kinetics, Chem. Rev. 109 (2009) 839–860.
[76] J.Y. Suh, C. Tang, G.M. Clore, Role of electrostatic interactions in transient encounter complexes in protein–protein association investigated by paramagnetic relaxation enhancement, J. Am. Chem. Soc. 129 (2007) 12954–12955.
[77] K. Sugase, H.J. Dyson, P.E. Wright, Mechanism of coupled folding and binding of an intrinsically disordered protein, Nature 447 (2007) 1021–1025.
[78] Z.X. Liang, J.M. Nocek, K. Huang, R.T. Hayes, I.V. Kurnikov, D.N. Beratan, B.M. Hoffman, Dynamic docking and electron transfer between Zn-myoglobin and cytochrome b_5, J. Am. Chem. Soc. 124 (2002) 6849–6859.
[79] J.A.R. Worrall, Y.J. Liu, P.B. Crowley, J.M. Nocek, B.M. Hoffman, M. Ubbink, Myoglobin and cytochrome b_5: a nuclear magnetic resonance study of a highly dynamic protein complex, Biochemistry 41 (2002) 11721–11730.
[80] S. Kuhlgert, F. Drepper, C. Fufezan, F. Sommer, M. Hippler, Residues psaB Asp612 and psaB G1u613 of Photosystem I confer pH-dependent binding of plastocyanin and cytochrome *c*(6), Biochemistry 51 (2012) 7297–7303